Original Paper

Effects of multi-scale wave-induced fluid flow on seismic dispersion, attenuation and frequency-dependent anisotropy in periodic-layered porous-cracked media

Zhao-Yun Zong [a, *], Yan-Wen Feng [b], Fu-Bin Chen [a, c], Guang-Zhi Zhang [a]

a
b
c

Received 5 May 2024
Received in revised form
5 July 2024
Accepted 11 November 2024
Available online 13 November 2024

Edited by Meng-Jiao Zhou

Wave-induced fluid flow
Multi-scale wave equations
Anisotropy
Dispersion and attenuation

The wave-induced fluid flow (WIFF) occurring in the ubiquitous layered porous media (e.g., shales) usually causes the appreciable seismic energy dissipation, which further leads to the frequency dependence of wave velocity (i.e., dispersion) and elastic anisotropy parameters. The relevant knowledge is of great importance for geofluid discrimination and hydrocarbon exploration in the porous shale reservoirs. We derive the wave equations for a periodic layered transversely isotropy medium with a vertical axis of symmetry (VTI) concurrently with the annular cracks (PLPC medium) based on the periodic-layered model and anisotropic Biot's theory, which simultaneously incorporate the effects of microscopic squirt fluid flow, mesoscopic interlayer fluid flow and macroscopic global fluid flow. Notably, the microscopic squirt shorten fluid flow emerges between the annular-shaped cracks and stiff pores, which generates one attenuation peak. Specifically, we first establish the stress-strain relationship and pore fluid pressure in a PLPC medium, and then use them to derive the wave equations by means of the Newton's second law. The plane analysis is implemented on the wave equations to yield the analytic solutions for phase velocities and attenuation factors of four waves, namely, fast P-wave, slow P-wave, SV-wave and SH-wave, and the anisotropy parameters can be therefore computed. Simulation results show that P-wave velocity have three attenuation peaks throughout the full frequency band, which respectively correspond to the influences of interlayer flow, the squirt flow and the Biot flow. Through the results of seismic velocity dispersion and attenuation at different incident angles, we find that the WIFF mechanism also has a significant impact on the dispersion characteristics of elastic anisotropy parameters within the low-mid frequency band. Moreover, it is shown that several poroelastic parameters, such as layer thickness ratio, crack aspect ratio and crack density have notable influence on seismic dispersion and attenuation. We compare the proposed modeled velocities with that given by the existing theory to confirm its validity. Our formulas and result can provide a better understanding of wave propagation in PLPC medium by considering the unified impacts of micro-, meso- and macro-scale WIFF mechanisms, which potentially lays a theoretical basis of rock physics for seismic interpretation.

of fractures in subsurface fractured media (Amalokwu et al., 2016; Li et al., 2018a, 2018b; Wei et al., 2013; Wang et al., 2018). Nevertheless, the quantitative seismic evaluation of reservoir is based on the comprehensive research of the intrinsic relationship between the physical properties of rocks and seismic attributes.

In order to establish the relationship between the rock physical properties and their dispersion and attenuation, a large quantity of attenuation theories for fluid-saturated poroelastic media are well established, which can be classified into three main categories ac-

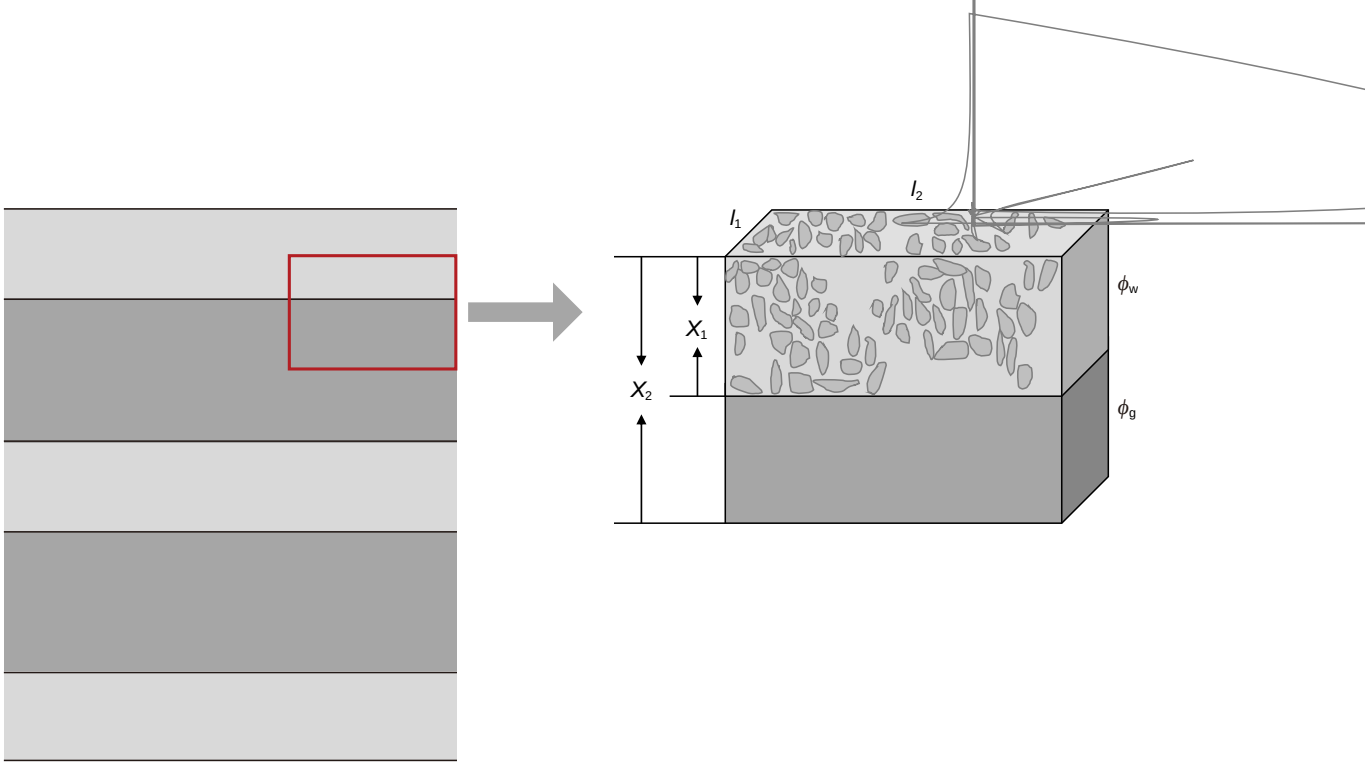

$$\begin{bmatrix} \sigma \\ \sigma \\ \sigma \\ \sigma \\ \sigma \\ \sigma \\ -\phi \end{bmatrix} = \begin{bmatrix} 11 & 12 & 13 & 14 & 15 & 16 & 17 \\ 12 & 22 & 23 & 24 & 25 & 26 & 27 \\ 13 & 23 & 33 & 34 & 35 & 36 & 37 \\ 14 & 24 & 34 & 44 & 45 & 46 & 47 \\ 15 & 25 & 35 & 45 & 55 & 56 & 57 \\ 16 & 26 & 36 & 46 & 56 & 66 & 67 \\ 17 & 27 & 37 & 47 & 57 & 67 & 77 \end{bmatrix} \begin{bmatrix} \\ \\ \\ \\ \\ \\ \Theta \end{bmatrix} \quad (1)$$

Eq. (1) is subjected to elementary deformation, and Θ is eliminated. Then, we can obtain

$$\sigma = \quad - \overline{\alpha} \quad (2)$$

where $\sigma = \left(\sigma \ , \sigma \ , \sigma \ , \sigma \ , \sigma \ , \sigma \ \right)^{\mathrm{T}}$ denotes the solid-phase stress tensor, $= (\ , \ , \ , \ , \ , \ )^{\mathrm{T}}$ denotes the solid-phase strain tensor, $= \ - \ _7/ \ _{77}(, = 1,2,\cdots,6)$ denotes drained elastic coefficients, and the coefficient vector $\overline{\alpha} = (\overline{\alpha}_1, \overline{\alpha}_2, \overline{\alpha}_3, \overline{\alpha}_4, \overline{\alpha}_5, \overline{\alpha}_6)^{\mathrm{T}}$, in which $\overline{\alpha} \ = \ _7\phi/ \ _{77}, \ = 1,2,\cdots,6,$ is the fluid pressure, and ϕ is porosity.

The total stress of the fluid-solid phase in this model can be expressed as

$$\begin{aligned} &\tau = \sigma \ - \phi \ \delta \ , \\ &\delta \ = 0, \neq ; \delta \ = 1, \ = \end{aligned} \quad (3)$$

Substituting Eq. (2) into Eq. (3) yields

$$\tau = \quad - \alpha \quad (4)$$

in which, $\alpha = \overline{\alpha} + \phi$, and is the unit matrix.

For porous VTI media, if the solid particles are assumed to be isotropic, the formula can be further simplified as

$$\begin{cases} \alpha_1 = \alpha_2 = 1 - \dfrac{_{11} + \ _{12} + \ _{13}}{3 \ _s} \\ \alpha_3 = 1 - \dfrac{_{13} + \ _{23} + \ _{33}}{3 \ _s} \\ \alpha_4 = \alpha_5 = \alpha_6 = 0 \end{cases} \quad (5)$$

in which, $_s$ represents the bulk modulus of solid grain. Thereby, the total stress of the novel model yields

$$\tau = \quad - \alpha \quad (6)$$

in which $\tau = (\tau \ , \tau \ , \tau \ , \tau \ , \tau \ , \tau \ )^{\mathrm{T}}$ denotes the total stress tensor, $= (\ , \ , \ , \ , \ , \ )^{\mathrm{T}}$ denotes the solid-phase strain tensor, is a 6×6 matrix of elastic constants, and $\alpha = (\alpha_1, \alpha_2, \alpha_3, \alpha_4, \alpha_5, \alpha_6)^{\mathrm{T}}$ is the porous elastic coefficient tensor.

To more precisely analyze the attenuation and dispersion of micro-scale seismic waves due to the squirt fluid flow, Tang (2011) proposed a unified theory of elastic wave in porous and cracked media. Vertically oriented cracks are introduced into the rock, and then an annular-shaped pore-crack structure is form with the stiff pores in the background of the porous medium. In the unit rock volume, the increment of fluid dilatation into the porous space due to local fluid flow is $_v$, and the pore pressure will also change accordingly with the added fluid content $\phi \ _v$. Thus, the constitutive equation for the pore fluid pressure is obtained (Tang et al., 2012):

$$= -(\alpha \nabla \cdot \mathbf{u} + \nabla \cdot \mathbf{w} + \phi \ _v)/\beta \quad (7)$$

where $\mathbf{w} = \phi(\mathbf{U} - \mathbf{u})$, $\mathbf{U}$ and $\mathbf{u}$ represent fluid displacement and

solid displacement respectively. $\beta = (\alpha - \phi)/\ _s + \phi/\ _f$, $_f$ represent the bulk modulus of pore fluid.

$(\omega) = \phi\ _v/$ are used to characterize the effect of squirt fluid flow caused by the annular cracks on pore pressure, respectively. Eq. (7) can be rewritten as

$$= -\frac{\phi}{\phi + \quad(\omega)}\left(\nabla\cdot\mathbf{U} + \frac{\alpha-\phi}{\phi}\nabla\cdot\mathbf{u}\right) \tag{8}$$

in which, $= (1/\ _f + 1/(\phi\ \ ))^{-1}$ is Biot-flow coefficient, $1/\ \ = \alpha - \phi/\ _s$.

The Biot-flow coefficient is also not identical in the -, -, - directions because of the directional effective stress. Thus, we define the Biot-flow coefficient tensor

$$= \begin{pmatrix} _1 & 0 & 0 \\ 0 & _2 & 0 \\ 0 & 0 & _3 \end{pmatrix} \tag{9}$$

where denotes the Biot-flow tensor element in the -direction, whose inverse $^{-1}$ reflects the compressibility of the Biot-flow to the solid-fluid coupled system, and

$$\begin{aligned} &= \left(\frac{1}{_f} + \frac{1}{\phi}\right)^{-1} \\ \frac{1}{\ } &= \frac{\alpha - \phi}{_s} \end{aligned} \tag{10}$$

In addition, the expressions for (ω) is

$$(\omega) = \frac{\frac{8(1-\nu_0)\ _c(1+\lambda)^3}{3\mu_0}\frac{1/\ _0 - 1/\ _s}{1/\ _d - 1/\ _0}\quad _c}{1 - \frac{3\ \omega\eta(1+2\lambda)}{2\ _f\lambda\gamma_c^2}\left[1 + \frac{4(1-\nu_0)\ _f(1+\lambda)^3}{3\pi\mu_0\gamma_c(1+2\lambda)}\quad _c\right]} \tag{11}$$

Parameter $_c$ is given by

$$_c = 1 + \frac{(4-5\nu_0)(\ /\ )^3}{2(7-5\nu_0)(1+\ /\ )^3} + \frac{9(\ /\ )^5}{2(7-5\nu_0)(1+\ /\ )^5} \tag{12}$$

in which, ν_0 is Poisson's ratio of background medium, μ and $_d$ represent the shear modulus and dry bulk modulus of solids, respectively, $_0$ is the bulk modulus of saturated rock without the squirt flow. $_c$ and γ_c are crack density and crack aspect ratio respectively. $\lambda = \ /\ = [3\phi/(4\pi\ _c)]^{1/3}$, is the radius of the circular hole, is the length of the crack. ω is frequency, and η is the fluid viscosity.

As the frequency tends to zero, (0) is a nonzero positive real number, which also leads to the low-frequency limit of the Tang's model constructed on the basis of the unified theory of micro-scale pore-crack media to be lower than the Gassmann limit. To correct this issue, the concept of dynamic bulk modulus was introduced (Yao et al., 2015). Therefore, the modified additional flexibility of the squirt flow $\Delta\ (\omega)$ is

$$\Delta\ (\omega) = \ (\omega) - \ (0) \tag{13}$$

in which $(0) = \frac{8(1-\nu_0)\ _c(1+\lambda)^3}{3\mu}\frac{1/\ _0 - 1/\ _s}{1/\ \ - 1/\ _0}$.

White (1975) used the ideal layered model of with periodic alternation of water and gas layers to simulate the partial saturation of mesoscopic inhomogeneous fluid. In the PLPC medium, only the interlayer fluid flow caused by seismic waves propagation along the direction perpendicular to the layer is considered. In the periodic-layered medium, the interlayer fluid pressure difference caused by two adjacent layers with different fluids will cause interlayer fluid flow and affect the average fluid pressure. In the following, we derive the expression of fluid pressure considering interlayer fluid flow.

Considering that the unit rock contains two-layer media, the P-wave modulus of plane wave can be written as (White, 1975)

$$_0 = \left(\frac{1}{_1} + \frac{2}{_2}\right)^{-1} \tag{14}$$

where

$$_1 = \frac{1}{2},\ _2 = \frac{2 - \ 1}{2} \tag{15}$$

$_1$ and $_2$ are the bulk modulus of P-wave in the upper and lower layers respectively, and

$$\begin{aligned} \ &= \overline{\ } + \ \left(1 - \frac{^*}{_s}\right)^2 \\ \overline{\ \ } &= \ ^* + \frac{4}{3}\mu_d \\ \ &= \left(\frac{\phi}{_f} + \frac{1-\phi}{_s} - \frac{^*}{_s^2}\right)^{-1} \\ ^* &= (\ _{11} + 2\ _{12} + 2\ _{13} + 2\ _{23} + \ _{22} + \ _{33})/9 \end{aligned} \tag{16}$$

In the research unit circled by the red frame in Fig. 1, when no fluid passes through the interface between the two layers, we assume that the pore fluid pressures of two-layer media are $_1e^{-,\omega}$ and $_2e^{-,\omega}$, respectively, which are expressed as a multiple of $_0$:

$$\begin{aligned} _1e^{-,\omega} &= \ _1\ _0e^{-,\omega} \\ _2e^{-,\omega} &= \ _2\ _0e^{-,\omega} \end{aligned} \tag{17}$$

Since $_1$ and $_2$ are different, a pressure gradient will be generated at the interface, which will cause the fluid to flow between the layers, that is, the interlayer fluid flow. The velocity of the interlayer fluid flow is

$$e^{-,\omega} = \frac{\ _1 - \ _2}{\ _1 + \ _2}e^{-,\omega} \tag{18}$$

in which, $_1$ and $_2$ represent the wave impedance in the upper and lower layers of the unit rock respectively, as follows,

$$\begin{aligned} _1 &= \ _{01}\coth(\ _1\ _1) \\ _2 &= \ _{02}\coth(\ _2(\ _2 - \ _1)) \end{aligned} \tag{19}$$

where $_0 = \sqrt{\eta\ _E/(\ \omega\ )}$, $\ = \sqrt{\ \omega\eta/(\ _E\ )}$, is the permeability. $_E$ denotes the effective bulk modulus in the upper and lower layers of the unit rock,

$$_E = \frac{\ }{\ \ \ \ } \tag{20}$$

Due to the interlayer fluid flow, the thickness of the two-layer medium changes dynamically. The variations are as follows:

$$\begin{aligned} U\ _1e^{-,\omega} &= \left(- \ \frac{1}{\ \omega}\right)e^{-,\omega} \\ U\ _2e^{-,\omega} &= \left(\ \frac{2}{\ \omega}\right)e^{-,\omega} \end{aligned} \tag{21}$$

where $/(\ \omega)$ is the displacement amplitude of the fluid flow

passing through the interface. The sum of the displacements is divided by the thickness to obtain the additional strain $_{f}$ due to interlayer fluid flow:

$$_{f}e^{-\omega} = \left(\frac{U_1 + U_2}{2}\right)e^{-\omega} \tag{22}$$

According to White's theory, $_1 = _1$ and $_2 = _2$, can be calculated as follows:

$$_1 = \left(1 - \frac{^*}{_s}\right)\frac{_1}{_1};\quad _2 = \left(1 - \frac{^*}{_s}\right)\frac{_2}{_2} \tag{23}$$

Finally, the additional strain $_f$ caused by the interlayer fluid flow can be obtained by substituting the calculated and Eqs. (17), (18) and (21) into Eq. (22).

Thus, the total average pore fluid pressure in the PLPC medium can be obtained:

$$= -\frac{\phi}{\phi + \left((\omega) + _f\right)}\left(\nabla\cdot\mathbf{U} + \frac{\alpha-\phi}{\phi}\nabla\cdot\mathbf{u}\right) \tag{24}$$

where $_f = _f/$ characterizes the effect of interlayer fluid flow on pore pressure.

The elastic kinetic equations based on microscopic fluid flow fields in porous anisotropic media are shown below:

$$\begin{cases} \frac{\partial\sigma}{\partial} + \frac{\partial\sigma}{\partial} + \frac{\partial\sigma}{\partial} = \frac{\partial^2}{\partial\ ^2}\left(\rho\ + \rho_f\ \right) \\ \frac{\partial\sigma}{\partial} + \frac{\partial\sigma}{\partial} + \frac{\partial\sigma}{\partial} = \frac{\partial^2}{\partial\ ^2}\left(\rho\ + \rho_f\ \right) \\ \frac{\partial\sigma}{\partial} + \frac{\partial\sigma}{\partial} + \frac{\partial\sigma}{\partial} = \frac{\partial^2}{\partial\ ^2}\left(\rho\ + \rho_f\ \right) \\ -\frac{\partial}{\partial} = \frac{\partial^2}{\partial\ ^2}\left(\rho_f\ + \sum\ \ \right) + \eta\sum\frac{1}{}\frac{\partial}{\partial} \end{cases} \tag{25}$$

in which $_{11} = \left(\phi\rho_f + \rho\ \right)/\phi^2$, $_{22} = \left(\phi\rho_f + \rho\ \right)/\phi^2$, $_{33} = \left(\phi\rho_f + \rho\ \right)/\phi^2$, $\rho = (1-\phi)\rho_s + \phi\rho_f = \rho_1 + \rho_2$, $\rho_1 = (1-\phi)\rho_s$, $\rho_2 = \phi\rho_f$, and $$ is the anisotropic permeability.

Substituting Eq. (6) into Eq. (25), the elastic wave propagation equation for periodic-layered porous-cracked media in general anisotropic conditions is obtained as follows:

$$\begin{cases} \frac{\partial}{\partial}\left(\ \ \frac{\partial}{\partial}\right) - \frac{\partial}{\partial}(\alpha\ \ ) = \frac{\partial^2}{\partial\ ^2}\left(\rho_1\ \ + \rho_2\ \ \right) \\ \\ -- \end{cases}$$

in which,

$$= \omega^2 \rho$$

Table 1
The rock physics parameters.

Parameter	Symbol	Value	Parameter	Symbol	Value
Grain bulk modulus	, GPa	37.9	Grain density	ρ_s, kg·m^{-3}	2650
Grain shear modulus	μ , GPa	32.6	Water density	ρ_f, kg·m^{-3}	1000
Water bulk modulus	$_f$, GPa	2.25	Gas density	ρ_g, kg·m^{-3}	70
Gas bulk modulus	$_g$, GPa	9.6×10^{-3}	Crack density	$_c$	0.025
Water viscosity	η_w, Pa·s	0.005	Crack aspect ratio	γ_c	0.0012
Gas viscosity	η_g, Pa·s	1×10^{-6}	Tortuosity	τ	2.4
Upper layer thickness	$_1$, m	0.1	Upper layer porosity	ϕ_w	0.25
Total thickness	$_2$, m	0.25	Sublayer porosity	ϕ_g	0.25
Coupling density	ρ , kg·m^{-3}	300	Permeability	, mD	10
	ρ , kg·m^{-3}	300		, mD	10
	ρ , kg·m^{-3}	100		, mD	20

3. Numerical example

In this section, we use the above method to calculate the dispersion, attenuation and frequency-dependent anisotropy of seismic waves in PLPC medium, and analyze the influence of different parameters on the dispersion and attenuation of seismic waves. Table 1 is the rock physics parameters to analyze the seismic wave theory.

The elastic modulus of the dry rock skeleton of the PLPC medium can be expressed as

$$\begin{aligned}
^0_{11} &= (\lambda_d + 2\mu_d) - \lambda_d^2 \Delta \quad \big/ (\lambda_d + 2\mu_d) \\
^0_{33} &= (\lambda_d + 2\mu_d)(1 - \Delta \quad) \\
^0_{13} &= \lambda_d (1 - \Delta \quad) \\
^0_{55} &= \mu_d (1 - \Delta \quad) \\
^0_{66} &= \mu_d
\end{aligned} \tag{43}$$

in which, $^0_{23} = {}^0_{13}$, $^0_{22} = {}^0_{11}$, $^0_{44} = {}^0_{55}$, $^0_{12} = {}^0_{11} - 2\,{}^0_{66}$, λ_d and μ_d are the Lamé constants of the dry rock, $\Delta \quad = 4\,{}_c/[3\,(1 - \quad)]$, $\Delta \quad = 16\,{}_c/[3(3 - 2\,\quad)]$, $\quad = \mu_d/(\lambda_d + 2\mu_d)$.

For fluid-containing anisotropic media, the generalized Gassmann equation can characterize the elastic modulus parameters of anisotropic media (Gassmann, 1951). Therefore, the elastic modulus of saturated rock in the three-scale model of the PLPC medium can be expressed as

$$\begin{aligned}
_{11} &= (\lambda + 2\mu) - \lambda^2 \Delta \quad \big/ (\lambda + 2\mu) + \alpha_{11}^2 \\
_{33} &= (\lambda + 2\mu)(1 - \Delta \quad) + \alpha_{33}^2 \\
_{13} &= \lambda (1 - \Delta \quad) + \alpha_{11}\alpha_{33} \\
_{55} &= \mu (1 - \Delta \quad) \\
_{66} &= \mu
\end{aligned} \tag{44}$$

in which, $_{23} = {}_{13}$, $_{22} = {}_{11}$, $_{44} = {}_{55}$, $_{12} = {}_{11} - 2\,{}_{66}$. is the Gassmann pore modulus,

$$= \frac{_s}{(1 - {}^*/{}_s) - \phi\left(1 - {}_s/{}_f\right)} \tag{45}$$

and * is generalized bulk modulus of dry rock,

$$^* = \frac{1}{9}\sum_{=1}^{3}\sum_{=1}^{3} {}^0_{} \tag{46}$$

The P-wave velocity dispersion and attenuation curves of the three-scale model of anisotropic media with pores and cracks (red curve and dark blue curve) are compared with those of the fast P-wave velocity dispersion and attenuation curves given by the Biot theory based on VTI media (navy blue curve), the Tang theory with penny-shaped cracks (light blue curve) and annular-shaped cracks (yellow curve) considering macroscopic global flow, and the White periodic layered media theory (orange curve) considering macroscopic global flow. The crack density of the penny-shaped cracks (crack 1) is 0.025, and the crack aspect ratio is 0.0017; the crack density of the annular-shaped cracks (crack 2) is 0.025, and the

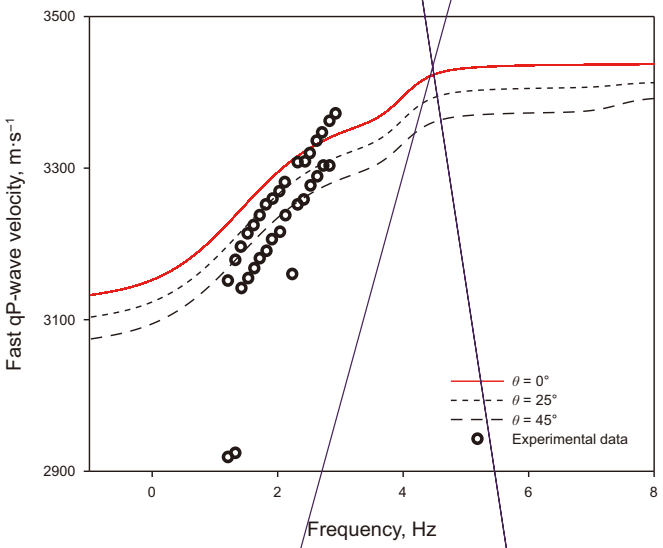

Fig. 6. Comparison of fast qP-wave velocities with experimental data.

of anisotropy, the velocity dispersion and attenuation of fast P-wave will change will change with the variation of the propagation angle, and this characteristic is the biggest difference between this theory and the theory of isotropic medium. The relative increase or decrease of the attenuation peak in different frequency bands may be due to the fact that different fluid flow mechanisms are not independent of each other. The interaction between them will affect the dispersion and attenuation caused by each WIFF mechanism.

To further investigate the rationality of the theory in this paper, we calculate the velocity curves of fast P-wave, slow P-wave and SV-wave with incident angle at frequencies of 0.8, 8 and 800 kHz. We assume that the incident angle θ is the angle between the propagation direction of the wave and the $$-axis. From Fig. 4, it is shown that the seismic wave velocity increases with the increase of frequency. Moreover, under the given medium model parameters, the velocities of fast P-wave and SV-wave show anisotropic characteristics. The SV-wave has its maximum velocity when its propagation direction is at an angle of 45° normal to the layer. The difference in the velocity values of the fast P-wave propagating along the parallel and perpendicular layer is not significant, which we attribute to the presence of interlayer fluid flow.

The Thomsen anisotropy parameters are calculated to better characterize the frequency-dependent anisotropy of seismic waves in PLPC medium, as follows (Thomsen, 1986):

$$\varepsilon^{(V)} = \frac{11 - 33}{2\ 33},$$
$$\delta^{(V)} = \frac{(13 + 44)^2 - (33 - 44)^2}{2\ 33(33 - 44)}. \tag{47}$$

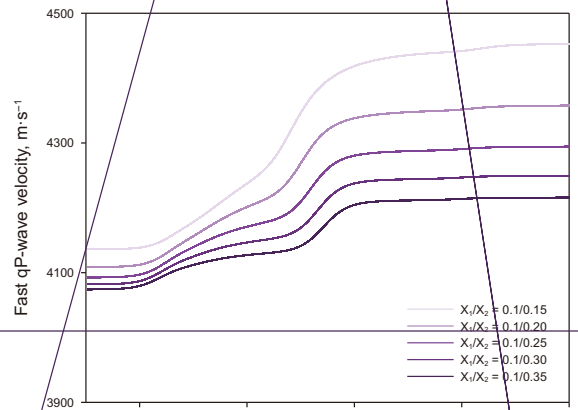

(a) Fast P-wave velocity

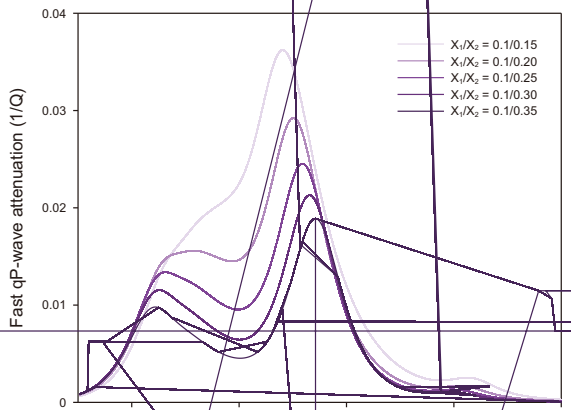

(b) Fast P-wave attenuation

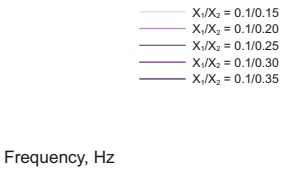

(c) SV-wave velocity

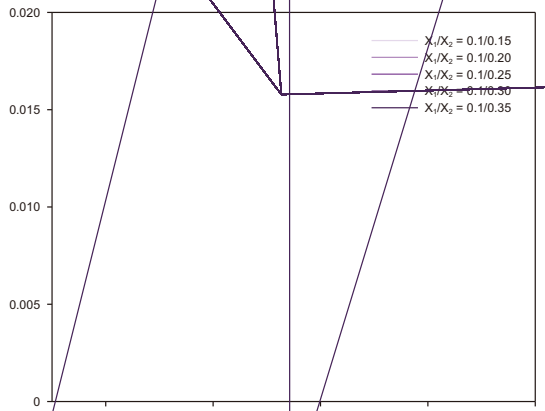

(d) SV-wave attenuation

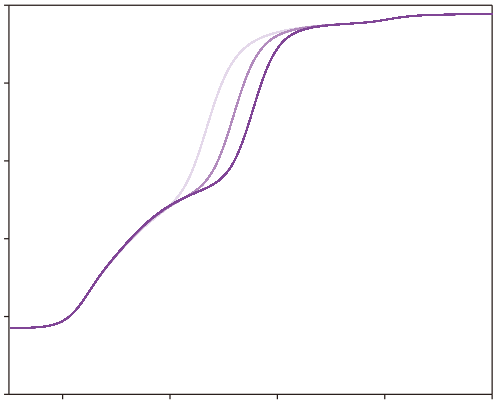

The characteristics of the Thomsen anisotropy parameters with frequency are analyzed for different crack densities, which are set at 0.1, 0.12, 0.14, 0.16 and 0.18, respectively. According to Fig. 5, the interlayer fluid flow and two kinds of squirt fluid flow will cause dispersion phenomenon to the anisotropic parameters in the frequency band below 10^4 Hz, which proves that the WIFF mechanism will also have a slight influence on the anisotropic parameters. Simultaneously, as the crack density increases, the anisotropic parameters also increase accordingly.

In order to verify the validity of the three-scale wave theory, a comparative analysis is conducted between the experimental data and the simulated fast P-wave velocities. The experimental data are fast P-wave velocities measured by low-frequency stress-strain experiments on water-saturated dense siltstone samples (Ba et al., 2017). The porosity of the tight siltstone is 0.14, the permeability is 0.084 mD, the rock background bulk modulus is 20 GPa, and the shear modulus is 11.8 GPa. The crack density of the annular-shaped crack in the model is set to 0.03, the crack aspect ratio is 0.002, the fluid viscosity is 0.001 Pa s, and the fluid bulk modulus is 2.25 GPa. From Fig. 6, the fast P-wave velocity dispersion phenomenon is obvious in the experimental data within the seismic frequency band of 10^1–10^3 Hz, and the theoretical P-wave velocity curve is consistent with the experimental data. The dispersion in the lower frequency band is caused by mesoscopic wave-induced flow, and the velocity curve shows multiple dispersion features. Therefore, the comparison of laboratory-measured velocities with theoretical predictions shows that the proposed three-scale wave-induced flow theory can better describe the frequency-dependent characteristics of the velocity.

Subsequently, the effects of different elastic parameters on the velocity dispersion and attenuation of the three seismic waves propagating along the -axis in the PLPC model are analyzed. The first is layer thickness ratio. We set the thickness of the upper layer to 0.1 m, and the thickness of the lower layer to 0.05, 0.10, 0.15, 0.20 and 0.25 m respectively. From Fig. 7, with the decrease of the layer thickness ratio, the attenuation value of the velocity shows an increasing trend. The variation of the layer thickness ratio has an effect on these WIFF mechanisms, with the attenuation frequency band of the squirt fluid flow shifting towards the low frequency direction, and the attenuation frequency band of the interlayer fluid flow and the global fluid flow shifting towards the high frequency direction.

As shown in Fig. 8, the dispersion attenuation under different crack aspect ratios is analyzed. The aspect ratios of the annular cracks in the upper and lower media are set to 0.008, 0.0012, 0.0016, 0.002 and 0.0024, respectively. The variation of the crack aspect ratio mainly affects the microscopic squirt fluid flow mechanism. With the increase of the crack aspect ratio, the velocity

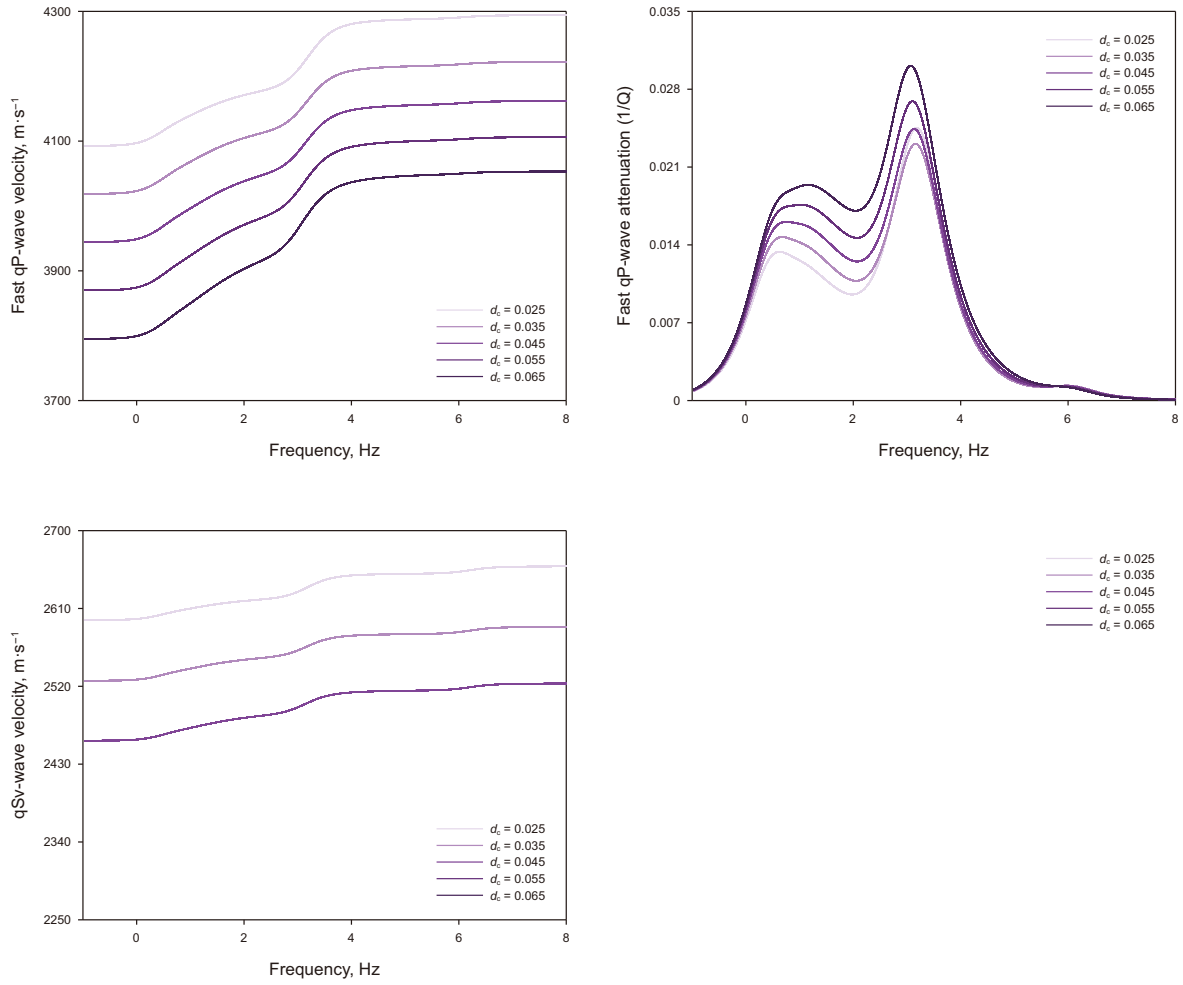

of two seismic waves decreases relatively, the attenuation frequency band moves to the high frequency direction, and the attenuation peak does not change significantly.

The crack density also has a significant effect on seismic wave velocity and dispersion. We set the crack densities of the annular-shaped cracks are 0.025, 0.035, 0.045, 0.055 and 0.065, respectively. According to Fig. 9, the crack density mainly affects the microscopic squirt fluid flow mechanism and the mesoscopic interlayer fluid flow mechanism. With the increase of crack density, the velocity of seismic wave decreases, the attenuation peak increases, and the attenuation frequency band is not affected.

Finally, we analyze the influence mechanism of different permeability on seismic wave velocity and dispersion. Here we set the permeability in the - and -axis directions to be 10, 20, 100, 200 and 400 mD, and the permeability in the -axis direction to be 5, 10, 50, 100 and 200 mD. As shown in Fig. 10, the variation of permeability has little effect on the total attenuation of seismic waves and mainly affects the mesoscopic interlayer fluid flow and macroscopic Biot fluid flow mechanisms. When the permeability increases, the attenuation peak characterizing the interlayer fluid flow moves to the high frequency direction, and the attenuation peak characterizing the Biot fluid flow moves to the low frequency direction.

4. Conclusion

In this work, a periodic-layered porous medium is modeled in which each layer is an anisotropic background saturated with different fluids and contains the annular-shaped cracks, termed as the PLPC medium model. This model incorporates three WIFF mechanisms: microscopic squirt fluid flow, mesoscopic interlayer fluid flow and macroscopic Biot fluid flow. By means of the Biot's poroelasticity theory, the wave equations are derived by constructing the constitutive matrix, fluid pressure equation and motion differential equation of the PLPC medium. By assuming the plane wave solution and solving the Christoffel equation, the corresponding seismic wave velocity and attenuation factor are obtained, and the Thomsen anisotropic parameters are further calculated. Subsequently, the velocity dispersion and attenuation of seismic waves due to multi-scale WIFF mechanisms are investigated at different incident angles. The analysis shows that three types of WIFF mechanisms are dominant on different frequency bands of seismic waves, and the interlayer fluid flow mechanism mainly occurs in the seismic frequency band, which has potential guiding significance for subsequent oil/gas identification and reservoir prediction. Meanwhile, the novel model also demonstrates the significant frequency-dependent anisotropy characteristics. The maximum dispersion of P-wave occurs in the direction perpendicular to the layer, while the maximum dispersion of SV-

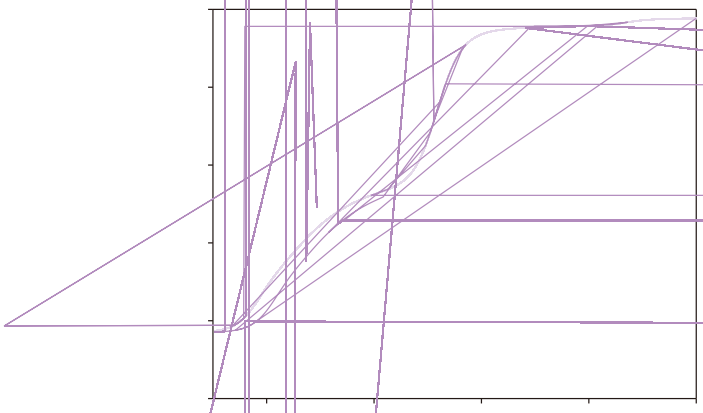

wave occurs in the direction with the incident angle of around 45°. The results show that the parameters such as layer thickness ratio, crack aspect ratio and crack density have an impact on the dispersion and attenuation of seismic waves. Each elastic parameter controls the WIFF mechanism differently, mainly affecting the attenuation peak, attenuation frequency band and velocity. Based on the proposed three-scale theoretical model, the influence of different elastic parameters on velocity dispersion, attenuation and frequency-dependent anisotropy characteristics can be analyzed to optimize sensitivity parameters for subsequent seismic reflection characteristics research. Furthermore, this study can also provide a theoretical basis for the matching of logging data and seismic data, thereby improving the effectiveness and stability of reservoir prediction.

CRediT authorship contribution statement

Zhao-Yun Zong: Writing – review & editing, Writing – original draft, Visualization, Validation, Software, Methodology, Investigation, Formal analysis, Conceptualization. **Yan-Wen Feng:** Writing – review & editing, Validation, Supervision, Resources, Methodology, Data curation, Conceptualization. **Fu-Bin Chen:** Writing – review & editing, Writing – original draft, Visualization, Validation, Supervision, Software, Methodology, Investigation, Formal analysis. **Guang-Zhi Zhang:** Liu Yang, Data curation, Funding acquisition, Resources, Validation, Writing – review & editing.

Data availability statement

The data underlying this article will be shared on reasonable request to the corresponding author.

Declaration of competing interest

The authors declare no conflict of interest.

Acknowledgements

The authors cordially thank the sponsorship of the National Natural Science Foundation of China (U24B2020, 42174139).

References

Amalokwu, K., Best, A.I., Chapman, M., 2016. Effects of aligned fractures on the response of velocity and attenuation ratios to water saturation variation: a laboratory study using synthetic sandstones. Geophys. Prospect. 64 (4), 942–957. https://doi.org/10.1111/1365-2478.12378.

Ba, J., Carcione, J., Nie, J., 2011. Biot-Rayleigh theory of wave propagation in double-porosity media. J. Geophys. Res. 116, B06202. https://doi.org/10.1029/2010JB008185.

Ba, J., Xu, W., Fu, L.Y., et al., 2017. Rock anelasticity due to patchy saturation and fabric heterogeneity: a double double-porosity model of wave propagation.

J. Geophys. Res. Solid Earth 122 (3), 1949–1976. https://doi.org/10.1002/2016JB013882.
Batzle, M., Han, D.H., Castagna, J.P., 2001. Fluids and frequency dependent seismic velocity of rocks. Geophysics 20, 5–8. https://doi.org/10.1190/1.1438900.
Biot, M.A., 1955. Theory of elasticity and consolidation for a porous anisotropic solid. J. Appl. Phys. 26, 182–185. https://doi.org/10.1063/1.1721956.
Biot, M.A., 1956a. Theory of propagation of elastic waves in a fluid-saturated porous solid. I. Low-frequency range. J. Acoust. Soc. Am. 28, 168–178. https://doi.org/10.1121/1.1908239.
Biot, M.A., 1956b. Theory of propagation of elastic waves in a fluid-saturated porous solid. II. Higher frequency range. J. Acoust. Soc. Am. 28, 179–191. https://doi.org/10.1121/1.1908241.
Chapman, M., 2003. Frequency-dependent anisotropy due to meso-scale fractures in the presence of equant porosity. Geophys. Prospect. 51, 369–379. https://doi.org/10.3997/2214-4609-pdb.5.P033.
Chapman, M., 2009. Modeling the effect of multiple sets of mesoscale fractures in porous rock on frequency-dependent anisotropy. Geophysics 74, D97–D103. https://doi.org/10.1190/1.3204779.
Chen, F.B., Zong, Z.Y., Yin, X.Y., 2022a. Acoustothermoelasticity for joint effects of stress and thermal fields on wave dispersion and attenuation. J. Geophys. Res. Solid Earth 127, e2021JB023671. https://doi.org/10.1029/2021JB023671.
Chen, Y., Zong, Z.Y., Zhu, H.J., 2022b. Biot-spherical squirt (BISSQ) model for wave attenuation and dispersion. Geophys. J. Int. 231 (2), 1138–1149. https://doi.org/10.1093/gji/ggac250.
Chen, F.B., Zong, Z.Y., Yin, X.Y., et al., 2023. Pressure and frequency dependence of elastic moduli of fluid-saturated dual-porosity rocks. Geophys. Prospect. 71, 1599–1615. https://doi.org/10.1111/1365-2478.13395.
Diallo, M.S., Prasad, M., Appel, E., 2003. Comparison between experimental results and theoretical predictions for P-wave velocity and attenuation at ultrasonic frequency. Wave Motion 37 (1), 1–16. https://doi.org/10.1016/S0165-2125(02)00018-5.
Dutta, N.C., Ode, H., 1979. Attenuation and dispersion of compressional waves in fluid-filled porous rocks with partial gas saturation (White model)—Part II: results. Geophysics 44, 1789–1805. https://doi.org/10.1190/1.1440939.
Dvorkin, J., Mavko, G., Nur, A., 1995. Squirt flow in fully saturated rocks. Geophysics 60, 97–107. https://doi.org/10.1190/1.1443767.
Gassmann, F., 1951. Elastic waves through a packing of spheres. Geophysics 16 (4), 673–685. https://doi.org/10.1190/1.1437718.
Guo, J.X., Han, T.C., Fu, L.Y., et al., 2019. Effective elastic properties of rocks with transversely isotropic background permeated by aligned penny-shaped cracks. J. Geophys. Res. Solid Earth 124, 400–424. https://doi.org/10.1029/2018JB016412.
Gurevich, B., Lopatnikov, S.L., 1995. Velocity and attenuation of elastic waves in finely layered porous rocks. Geophys. J. Int. 121, 933–947. https://doi.org/10.1111/j.1365-246X.1995.tb06449.x.
Gurevich, B., Makarynska, D., de Paula, O.B., et al., 2010. A simple model for squirt-fl